Structure, dielectric and magnetodielectric properties of $Bi_{1-x}Gd_xFeO_3$ Ceramics*

Li Jing-Bo(李静波)[a)†], Rao Guang-Hui(饶光辉)[a)], Xiao Yin-Guo(肖荫果)[b)], Luo Jun(骆 军)[a)], Liu Guang-Yao(刘广耀)[a)], Chen Jing-Ran(陈景然)[a)], and Liang Jing-Kui(梁敬魁)[a)c)]

[a)] *Beijing National Laboratory for Condensed Matter Physics, Institute of Physics, Chinese Academy of Sciences, Beijing* 100190, *China*

[b)] *Institut fuer Festkoerperforschung, Forschungszentrum Juelich, D*-52425 *Juelich, Germany*

[c)] *International Centre for Materials Physics, Chinese Academy of Sciences, Shenyang* 110016, *China*

(Received 28 April 2010; revised manuscript received 12 June 2010)

Different magnetodielectric effects were observed in $Bi_{1-x}Gd_xFeO_3$ ceramics depending on gadolinium content. A positive one was observed in the samples with $x \leq 0.10$ at 295 K and 16 K, and a negative one in the sample with $x = 0.4$ at 16 K. Structure analysis by x-ray diffraction (XRD) reveals that the samples crystallize in the *R*3*c* structure (ferroelectrics) for $x < 0.08$ and in the *Pbnm* structure (paraelectrics) for $x \geq 0.3$ at room temperature. Temperature-dependent dielectric response and x-ray diffraction confirm the occurrence of a structural transition in the *Pbnm* phase at low temperature for the samples with $x \leq 0.4$. While the positive magnetodielectric effects can be attributed to a coupling of magnetic and crystallographic structures of the *R*3*c* phase, the observed negative magnetodielectric effect in the *Pbnm* phase can be associated with a low-temperature modification of the *Pbnm* structure. The observed dual-signed magnetodielectric effects suggest that the $Bi_{1-x}Gd_xFeO_3$ oxides are a good prototype for understanding the magnetodielectric coupling mechanism in this kind of materials.

Keywords: multiferroic, magnetodielectric effect, x-ray diffraction, $Bi_{1-x}Gd_xFeO_3$ ceramics

PACC: 7580, 6100M, 7240

1. Introduction

Multiferroic materials that simultaneously exhibit ferroelectric and magnetic orders are currently gaining more and more attention of researchers, not only owing to the expectation that multiferroics would offer potential applications for devices taking advantage of the multiferroic coupling, but also to the interesting physics manifested by these materials.[1] $BiFeO_3$ (BFO) is one of the most studied magnetoelectric materials because its ferroelectric and antiferromagnetic orders present simultaneously above room temperature. The BFO compound crystallizes in an *R*3*c* structure. The G-type antiferromagnetic ordering takes place at about 640 K (T_N), while ferroelectric order appears at about 1100 K (T_{EC}).[2] The antiferromagnetic spin configuration of BFO is modified by superimposing on it a spiral modulated spin structure (SMSS) (620 Å periodicity, 1 Å=0.1 nm)[3] which gives rise to a cancellation of macroscopic magnetization and prohibits the linear magnetoelectric (ME) effect from being observed.[4] Despite the weak ME effect in bulk BFO, the antiferromagnetic domain switching by external electric field in BFO films highlights the possibility of application of BFO in modern electronic devices.[5] However, there exist some problems for the application of BFO, e.g. the large leakage current,[6] the large mismatch stress in the interface between BFO films and substrates, and the reduction of ME by the SMSS in the bulk and thick films. Element substitution can suppress the electric leakage[6] and the spiral spin structure to make the macroscopic magnetization and linear magnetoelectric effect observable,[4] as well as adjust the lattice parameters. At present, the driving mechanism of the ME coupling has not been fully understood. Although the observed ME effects were generally attributed to the coupling between ferroelectric and ferromagnetic order parameters,[7] first-principle calculations indicated that the weak magnetism was independent of the polarization distortion in BFO.[8,9] Under an external electric field, one kind of magnetoelectric coupling mechanism was revealed by observing the changes in

*Project supported by the National Basic Research Program of China (Grant No. 2007CB925003) and the National Natural Science Foundation of China (Grant No. 50872148).

†Corresponding author. E-mail: jbli@aphy.iphy.ac.cn

© 2010 Chinese Physical Society and IOP Publishing Ltd

the ferroelectric and antiferromagnetic domain structures of an epitaxial $BiFeO_3$ film.[5] The 109° ferroelectric switching (between the main polarization axis and the minor polarization axis) instead of the 180° switching (along the main polarization axis) can lead to a re-orientation of the antiferromagnetic easy plane to which the polarization axis is perpendicular. However, under a magnetic field which generally cannot change the antiferromagnetic easy plane due to the large superexchange energy, the route of the ME coupling remains in doubt.[8,9] It is known that the ferroelectric distortion of BFO mainly results from the hybridization between Bi s and O s/p orbits to form a localized lobe of the Bi^{3+} 6s lone pair electrons.[10] Substitution of rare earth elements (RE) for Bi would weaken the hybridization of the 6s electrons and affect the ligand field of Fe ions. A carefully investigation of the changes of structural distortions and physical properties caused by the RE substitution will be of benefit to understanding the spin–lattice interaction. In this paper the effects of Gd substitution for Bi on the crystal structure, magnetism, polarization and magnetodielectric (MDE) effect of the BFO were investigated. Interestingly, a positive MDE effect was observed in the samples with $x \leq 0.10$ at both 295 K and 16 K, whereas a negative MDE effect was observed in the sample with $x = 0.4$ at 16 K.

2. Experiment

$Bi_{1-x}Gd_xFeO_3$ ceramic samples with $x = 0$, 0.05, 0.08, 0.10, 0.15, 0.20, 0.25, 0.3, 0.4 and 0.5 were synthesized by a rapid sintering and quenching technique. Pre-dried starting materials of Bi_2O_3, Fe_2O_3, and Gd_2O_3 (purity > 99.9%) in stoichiometric proportions were thoroughly mixed and precalcined at 750 °C for 2 h. Then the mixture was ground and cold pressed into pellets and sintered at different temperatures for the samples with different Gd contents: 830 °C for BFO with an increment of 20 °C for every 10 at% Gd. One sintering cycle is 25 min, followed by a quenching process. Phase identification of the samples was carried out by x-ray powder diffraction using a Rigaku D/max 2500 diffractometer. The temperature dependent XRD analysis was performed using the Huber G670 diffractometer with a low-temperature accessory below room temperature. The microstructure of sintered samples was observed by scanning electron microscopy (SEM) using Hitachi S-5200. Pellets were coated by vaporizing Ag for electric investigations. The impedance investigation was performed by an NF ZM2353-LCR meter. Magnetic properties were studied by using a superconducting quantum interference device magnetometer (MPMS 7, SQUID).

3. Results and discussion

3.1. Experimental results

The x-ray diffraction (XRD) analysis exhibits that the $Bi_{1-x}Gd_xFeO_3$ samples crystallize in the perovskite structure (details in our previous paper[11]). The SEM observation of the fractured surface of the $Bi_{1-x}Gd_xFeO_3$ samples shows that the samples consist of two size grains, which might result from the semi-liquid phase sintering due to the fact that the sintering temperature is higher than the melting point of Bi_2O_3 ($\sim$ 825 °C[12]). Figure 1 shows the SEM images of the $Bi_{1-x}Gd_xFeO_3$ samples with $x = 0.05$, 0.20 and 0.40.

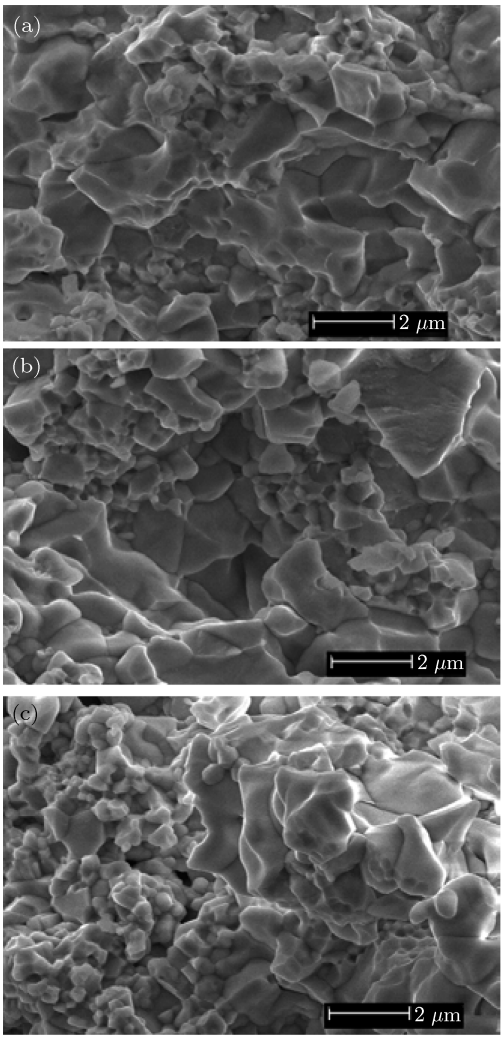


Fig. 1. SEM micrographs of the fractured surfaces of the $Bi_{1-x}Gd_xFeO_3$ ceramics with $x = 0.05$ (a); 0.20 (b); and 0.40 (c).

Rietveld refinement of the full XRD patterns was conducted by using the program FullProf.[13] Diffraction profile is modeled by the Thomposon-Cox-Hastings pseudo-Voigt function. For $x < 0.08$, the XRD patterns of the samples can be well fitted using the $R3c$ structure. For $x \geq 0.3$, the $Pbnm$ structure fits the XRD patterns satisfactorily. In the intermediate composition region, the XRD patterns of the samples can be fitted by the two-phase model of $R3c + Pbnm$. The $R3c$ phase is ferroelectric, whereas the $Pbnm$ structure does not have ferroelectric character due to its centrosymmetry. Table 1 lists the refined structural parameters of $R3c$ for $x \leq 0.1$. Figure 2 shows the composition dependences of volume fractions of $R3c$ and $Pbnm$ in samples, which were obtained from Rietveld refinement.

Table 1. Structural parameters of $R3c$ H for $Bi_{1-x}Gd_xFeO_3$ with $x = 0.0$, 0.05, 0.08 and 0.10 obtained from Rietveld refinement.

	$Bi_{1-x}Gd_xFeO_3$			
	x=0.0	x=0.05	x=0.08	x=0.10
a/Å	5.5785(3)	5.5762(3)	5.5706(3)	5.5693(4)
c/Å	13.8683(4)	13.8484(4)	13.8262(4)	13.8186(5)
V/Å^3	373.76(2)	372.91(2)	371.57(2)	371.19(3)
Bi/Gd: B/Å^2	0.47(2)	0.50(2)	0.47(2)	0.48(3)
Fe: z	0.2221(2)	0.2222(2)	0.2222(1)	0.2223(2)
B/Å^2	0.12(3)	0.13(3)	0.11(3)	0.12(3)
O_1: x	0.4526(15)	0.4460(14)	0.4424(12)	0.4403(18)
y	0.0200(16)	0.0209(15)	0.0214(12)	0.0216(15)
z	0.9493(6)	0.9555(6)	0.9580(5)	0.9588(6)
B/Å^2	0.89*	0.89*	0.89*	0.89*
the shortest Bi–O bond/Å	2.232(23)	2.295(23)	2.320(20)	2.328(28)
P_s	0.0370(6)	0.0306(7)	0.0281(8)	0.0273(10)
2α	21.3(3)	23.7(4)	25.1(5)	25.8(6)
R_{wp}/R_{exp}	13.8/7.4	10.2/7.1	12.8/7.0	12.5/7.0

Atoms are located in the $R3c$ H space group as follows: Gd/Bi at 6a: 0 0 0; Fe at 6a: 0 0 z; O at 18b: x y z.

* The temperature factor B of O in $R3c$ H from Ref. [14].

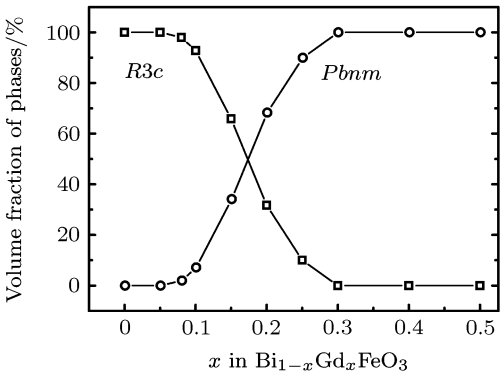


Fig. 2. The composition dependences of volume fractions of $R3c$ and $Pbnm$ in $Bi_{1-x}Gd_xFeO_3$ ceramics.

The $R3c$ structure can be regarded to evolve from the ideal cubic perovskite structure $Pm3m$ with two kinds of distortions: i) the ferroelectric distortion along the [111] axis of the cubic perovskite structure, resulting in $Pm3m \rightarrow R3m$ with the shortest Bi–O bond, as depicted in Fig. 3; ii) the relative rotation of two oxygen octahedra in the opposite direction around [111] with the rotation angle 2α, resulting in $Pm3m \rightarrow R\bar{3}c$ or $R3m \rightarrow R3c$.[8] Deduced from the structural parameters of the $R3c$ phases, the lattice polarization P_s and the relative rotation angle 2α are obtained in Table 1. Where, the P_s is defined as a ratio of the distance between the charge-centres of positive ions and negative ions along the polarization [111] axis to the lattice length along [111] in the $R3c$ unit-cell. The P_s decreases with increasing the Gd content, whereas the composition dependence of the angle 2α exhibits an opposite variation. The decrease of P_s is consistent with the concept that the substitution of Gd for Bi weakens the hybridization between Bi and O. The increase of 2α contributes to the increase of the weak magnetization of the samples containing the $R3c$ phase with the Gd content, as discussed in Ref. [11]. The structural analysis reveals that the length of the shortest Bi–O bonds contributes most to the hybridization between Bi and O increases

with increasing the Gd content, as listed in Table 1.

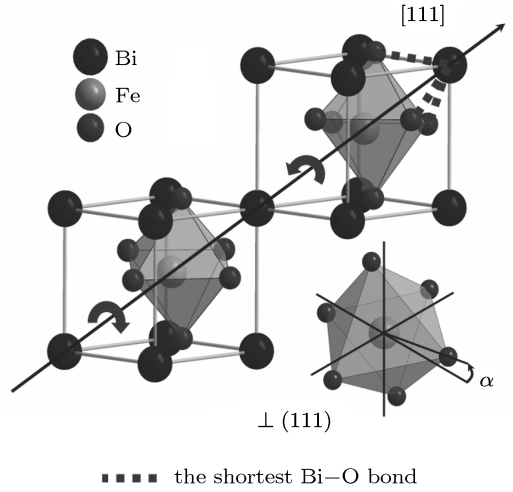


Fig. 3. Illustration of the structural distortions that lead to the *R*3*c* structure from two cubic perovskite unit cells: the ferroelectric distortion along the [111] axis and the relative rotation of oxygen octahedra in opposite directions around [111] with the relative rotation angle 2α.

The dielectric constant (ε') of the samples with $x \leq 0.3$ at room temperature varies in a range from 60 to 100 depending on the composition (Fig. 4), which is of the same magnitude as reported in Refs. [15] and [16]. The dielectric losses ($\tan\delta$) of the samples are less than 3%, indicating high insulation of the samples. For the samples with $x = 0.4$ and 0.5, both the dielectric constant and dielectric loss at room temperature are large and show strong frequency-dependence, showing large electric leakage in the materials. The observed dielectric response vs. temperature exhibits the presence of dielectric anomalies for the samples with $x \geq 0.15$, as shown in Fig. 5.

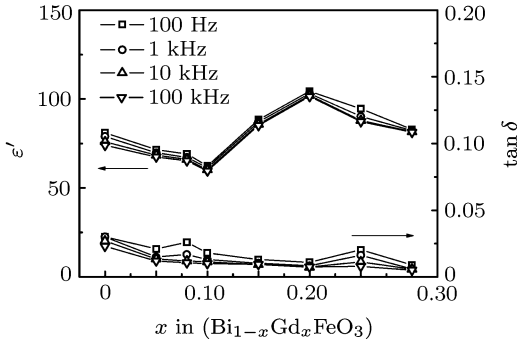


Fig. 4. The composition dependence of the dielectric constant ε' and loss $\tan\delta$ of $Bi_{1-x}Gd_xFeO_3$ ceramics with $x \leq 0.3$ at room temperature.

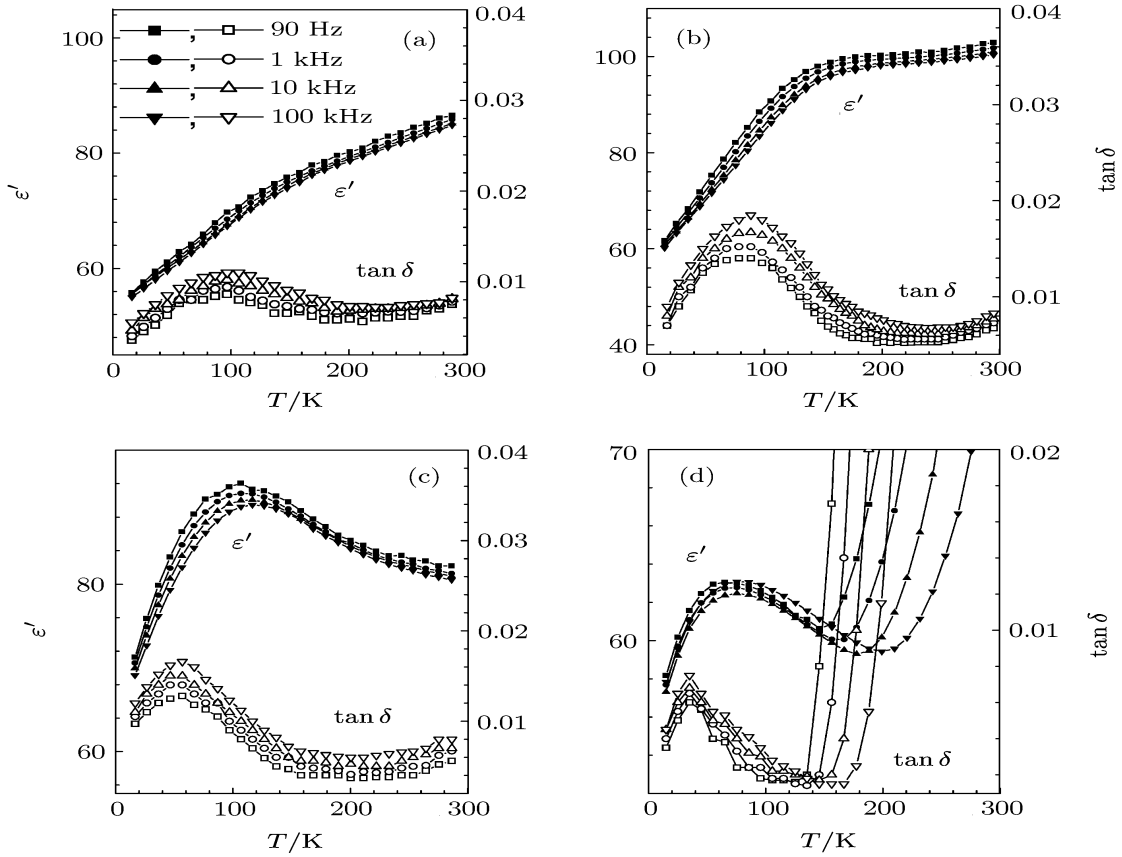


Fig. 5. Temperature dependence of dielectric response of $Bi_{1-x}Gd_xFeO_3$ samples with $x = 0.15$ (a); 0.20 (b); 0.30 (c); and 0.40 (d).

The dielectric anomalies indicate an occurrence of a phase transition of the *Pbnm* phase at low temperature. The transition temperature decreases with increasing the Gd content. Above 130 K, the dielectric constant and loss of the sample with $x = 0.40$ show steep increase with temperature and strong frequency dependence, indicating large electric leakage in the sample above 130 K. Below 130 K, the dielectric loss is less than 1%, showing good insulation of the sample with $x = 0.40$.

Temperature-dependent XRD measurements revealed that the low-temperature dielectric anomalies correspond to a structural transition of the *Pbnm* phase.[11] Figure 6 shows the temperature dependences of lattice parameters of the *Pbnm* phase for the sample with $x = 0.40$, which exhibit inflexions at low temperature in consistence with the dielectric anomalies.

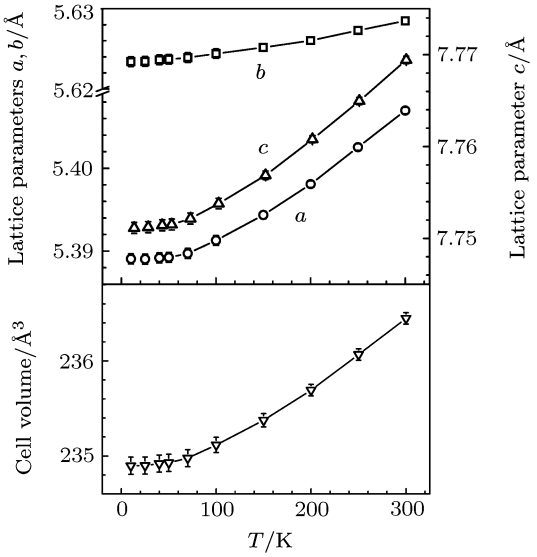


Fig. 6. Temperature dependences of lattice parameters of the *Pbnm* phase in the sample with $x = 0.40$.

The MDE effect was investigated by measuring the dielectric response under magnetic field using a ZM2353 LCR meter and a SQUID. Figure 7 shows the weak MDE effect, $\Delta\varepsilon$ ($\Delta\varepsilon = (\varepsilon_H - \varepsilon_0)/\varepsilon_0$) versus H, observed in $Bi_{1-x}Gd_xFeO_3$ with $x = 0$, 0.05, 0.10 and 0.40 at different temperatures. The values are much smaller than those ($\Delta\varepsilon \sim 0.6\%$ at 50 kOe, 1 Oe=80 A/m) resulting from the magnetoresistance and Maxwell–Wagner effect.[17] The samples with $x \leq 0.10$ which are, or mainly, composed of the *R*3*c* phase exhibit a positive MDE effect at both 16 K and 295 K as shown in Figs. 7(a)–7(d), but the sample with $x = 0.4$ exhibits a negative MDE effect at 16 K (Fig. 7(e)). Above the transition temperature of the *Pbnm* phase no apparent MDE was observed in the samples with $x = 0.4$ (Fig. 7(e)). The substitution of Gd for Bi enhances the MDE effect of the *R*3*c* phase as shown in Fig. 7(f), which depicts the variation of the $\Delta\varepsilon$ measured at 50 kOe and 295 K with the Gd content. In the two-phase region of $0.15 \leq x \leq 0.25$, a temporal relaxation of capacitance[17] occurs under an external magnetic field, which exhibits that the capacitance slowly decreases with time under the external magnetic field and prevents the observation of the intrinsic MDE effect. The temporal relaxation of capacitance was also observed on the sample with $x = 0.4$ in a narrow temperature region around the dielectric peak temperature (Fig. 5(d)). The capacitance relaxation observed in the two-phase samples might result from the enhanced local electrical inhomogeneity due to the existence of different phases in one sample. All the MDE measurements were repeated several times to ascertain the observations with the magnetic field parallel and perpendicular to the plate capacitances, respectively. It was found that the MDE values were reduced as H was parallel to E due to the large demagnetization factor resulting from the shape anisotropy, but the sign of $\Delta\varepsilon$ did not change. It is worth while noting that no apparent change of the dielectric loss was observed during the MDE measurements, suggesting an absence of magnetoresistance effect[17,18] in our samples.

The negative MDE effect in the sample with $x = 0.4$ was only observed at temperature below the low-temperature transition of the *Pbnm* phase. Above the transition temperature, no apparent MDE effect was observed, which is coincident with the fact that the sample crystallizes in the paraelectric *Pbnm* phase above the dielectric peak. The results suggest that the *Pbnm*-modification at low temperature is ferroelectric. Recently, Tokunaga *et al.*[19] reported that $GdFeO_3$ possessed a ferroelectric structure below ~ 2.5 K and the ferroelectric polarization in $GdFeO_3$ resulted from the exchange-interaction striction between two antiferromagnetic sublattices of Gd^{3+} and Fe^{3+} due to the occurrence of the antiferromagnetic order of Gd^{3+} at low temperature. However, the exchange-interaction striction mechanism could not take effect in our investigated samples due to the high transition temperature and lower Gd content in the samples. The ferroelectric distortion of the low-temperature *Pbnm*-modification might result from the hybridization of the Bi 6s lone-pair electrons with the s/p orbits of oxygen, as discussed in Ref. [11].

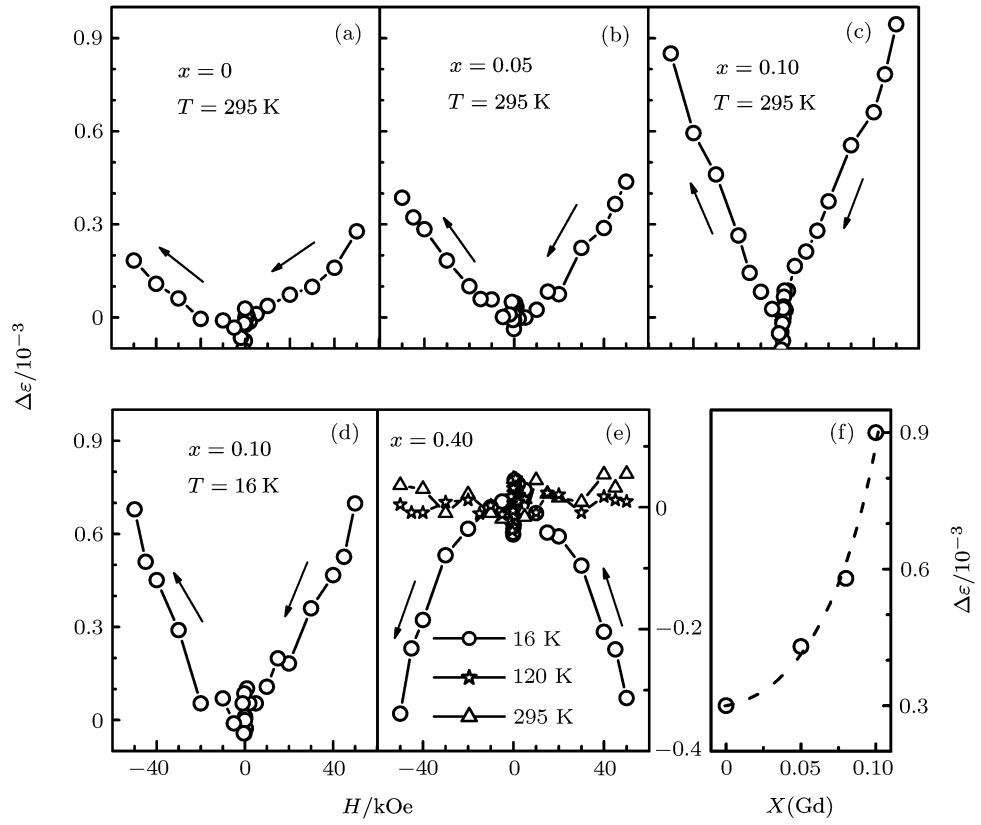


Fig. 7. Magnetodielectric effect, $\Delta\varepsilon$ versus H observed in $Bi_{1-x}Gd_xFeO_3$ with $x = 0$, 0.05 and 0.1 at 295 K, (a), (b), (c), respectively; $x = 0.1$ at 16 K, (d); $x = 0.4$ at 16 K, 120 K and 295 K, (e) ($f = 100$ kHz); and the composition dependence of $\Delta\varepsilon$ measured at 50 kOe and 295 K, (f). $\Delta\varepsilon$ was calculated by $(\varepsilon - \varepsilon_0)/\varepsilon_0$ (ε_0 is the ε as H is unloaded down to 0 from 50 kOe). The arrows show the loading route of H.

3.2. Discussion on magnetodielectric effect

In the G-type antiferromagnetic structure of BFO, the Fe magnetic moments are coupled ferromagnetically within the pseudocubic (111) planes and antiferromagnetically between adjacent planes. The weak ferromagnetism is symmetrically allowed as the magnetic moments are oriented perpendicular to the [111] direction in the $R3c$ structure and is caused by an antisymmetric spin coupling, namely the Dzyaloshinskii–Moriya (DM) interaction arising from the interplay between superexchange and spin–orbit coupling.[20] Ederer and Spaldin suggested that the weak DM magnetic moment $\boldsymbol{M}$ was directly related to the relative rotation of the two oxygen octahedra in the $R3c$ unit cell around the polarization [111] axis,[8] but independent of the polarization distortion in BFO.[8,9] However, our structural analysis reveals that the interaction between spin and lattice should exist in BFO via the rotation of the oxygen octahedra.

Under an external magnetic field (H), the weak ferromagnetic moments are enhanced due to the energy gain of the DM interaction, and tend to align with the applied field H. Because the weak ferromagnetism is strongly associated with the rotation of the oxygen octahedra,[8,9] the enhanced weak ferromagnetism indicates an increase of the relative rotation of the oxygen octahedra through the spin–orbit coupling. The increase of the relative rotation of the oxygen octahedra around the polarization [111] axis will decrease the length of the Bi–O bond and the rhombohedral angle, and increase the distortion along the polarization [111] axis, which corresponds to a decrease of the cell parameter a and an increase of c in the hexagonal $R3c$ H setting. The investigation of temperature-dependent spontaneous polarization of BFO suggested that the polarization was scaled by the c/a ratio.[21] Therefore, it can be concluded that the external magnetic field does increase the polarization in BFO through the DM interaction. The ME investigations on a single crystal of BFO using a pulsed magnetic field up to 280 kOe showed positive ME effect under most kind of $\boldsymbol{P}$–H-cell axis configurations,[22] supporting the above conclusion.

For the negative MDE effect in the sample with $x = 0.4$ at 16 K, it might be related to the different rotation mode or distortion of the oxygen octahedra in the low-temperature *Pbnm* modification. A further investigation on the detailed crystal structure of the low-temperature *Pbnm* modification is required for understanding the mechanism of the negative MDE effects.

4. Conclusions

In summary, the XRD analysis reveals that the samples $Bi_{1-x}Gd_xFeO_3$ with $x < 0.08$ are composed of the single-phase of *R*3c and those with $x \geq 0.30$ are the single-phase of *Pbnm*. Temperature-dependent dielectric response and XRD indicate a structural transition occurred in the *Pbnm* phase for the samples with $x \leq 0.4$ at low temperature. A weak positive MDE effect has been observed in samples with $x \leq 0.10$, while a weak negative MDE effect has been found in samples with $x = 0.3$ and 0.4 at 16 K. The positive MDE effect can be attributed to a coupling of magnetic and crystallographic structures of the *R*3*c* phase.

References

[1] Cheong S W and Mostovoy M 2007 *Nature Mater.* **6** 13

[2] Fischei P, Polemska M, Sosnowska I and Szymanski M 1980 *J. Phys.* C **13** 1931

[3] Sosnowska I, Peterlin-Neumaier T and Steichele E 1982 *J. Phys.* C **15** 4835

[4] Zaleskii A V, Frolov A A, Khimich T A and Bush A A 2003 *Phys. Solid State* **45** 141

[5] Zhao T, Scholl A, Zavaliche F, Lee K, Barry M, Doran A, Cruz M P, Chu Y H, Ederer C, Spaldin N A, Das R R, Kim D M, Baek S H, Eom C B and Ramesh R 2006 *Nature Mater.* **5** 823

[6] Yu B F, Li M T, Wang J, Pei L, Guo D Y and Zhao X Z 2008 *Physica* D: *Appl. Phys.* **41** 185401

[7] Palkar V R, Kundaliya D C, Malik S K and Bhattacharya S 2004 *Phys. Rev.* B **69** 212102

[8] Ederer C and Spaldin N A 2005 *Phys. Rev.* B **71** 060401R

[9] Ederer C and Fennie C J 2008 *J. Phys.: Condens. Matter* **20** 434219

[10] Ravindran P, Vidya R, Kjekshus A and Fjellvag H 2006 *Phys. Rev.* B **74** 224412

[11] Li J B, Rao G H, Xiao Y, Liang J K, Luo J, Liu G Y and Chen J R 2010 *Acta Mater.* **58** 3701

[12] Liu Y H, Li J B, Liang J K, Luo J, Ji L N, Zhang J Y and Rao G H 2008 *Mater. Chem. Phys.* **112** 239

[13] Rodriguez-Carvajal J 1993 *Physica* B **192** 55

[14] Sosnowska I, Schaefer W, Kockelmann W, Andersen K H and Troyanchuk I O 2002 *Appl. Phys.* A **74** S1040

[15] Jiang Q H, Ma J, Lin Y H, Nan C W, Shi Z and Shen Z J 2007 *Appl. Phys. Lett.* **91** 022914

[16] Eerenstein W, Morrison F D, Dho J, Blamire M G, Scott J F and Mathur N D 2005 *Science* **307** 1203a

[17] Kamba S, Nuzhnyy D, Savinov M, Sebek J, Petzelt J, Prokleska J, Haumont R and Kreisel J 2007 *Phys. Rev.* B **75** 024403

[18] Catalan G 2006 *Appl. Phys. Lett.* **88** 102902

[19] Tokunaga Y, Furukawa N, Sakai H, Taguchi Y, Arima T H and Tokura Y 2009 *Nature Mater.* **8** 558

[20] Moriya T 1960 *Phys. Rev.* **120** 91

[21] Ismailzade I G 1971 *Phys. Stat. Sol.* B **46** K39

[22] Popov Y F, Kadomtseva A M, Vorobev G P and Zvezdin A K 1994 *Ferroelectrics* **162** 135